Mild and Selective Hydrogenation of Nitrate to Ammonia in the Absence of Noble Metals

Lin Wei,[1] Da-Jiang Liu,[2] Bryan A. Rosales,[1] James W. Evans,[2,3] Javier Vela*[,1,2]

[1]Department of Chemistry, Iowa State University, [2]Ames Laboratory, [3]Department of Physics & Astronomy, Iowa State University, Ames, Iowa 50011, USA

KEYWORDS. Nitrate removal, nitrate reduction, catalytic hydrogenation, Ni_2P catalysts, non-precious metal, noble metal-free, high selectivity, ammonia.

ABSTRACT: Motivated by increased awareness about nitrate contamination of surface waters and its deleterious effects in human and animal health, we sought an alternative, non-noble metal catalyst for the chemical degradation of nitrate. First-row transition metal phosphides recently emerged as excellent alternatives for hydrogen evolution and hydrotreating reactions. We demonstrate that a key member of this family, Ni_2P readily hydrogenates nitrate (NO_3^-) to ammonia (NH_3) near ambient conditions with very high selectivity (96%). One of the few non-precious metal-based catalysts for this transformation, and among *ca.* 1% of catalysts with NH_3 selectivity, Ni_2P can be recycled multiple times with limited loss of activity. Both nitrite (NO_2^-) and nitric oxide (NO) intermediates are also hydrogenated. Density functional theory (DFT) indicates that—in the absence of a catalyst—nitrite hydrogenation is the reaction bottleneck. A variety of adsorbates (H, O, N, NO) induce surface reconstruction with top-layer Ni-rich surface stoichiometry. Critically, H saturation coverage on $Ni_2P(001)$ is only *ca.* 3 nm^{-2}, significantly less than that on Pd(111) and Ni(111) of *ca.* 15-18 nm^{-2}, which may play a key role in allowing coadsorption of NO_x. The ability of Earth-abundant, binary metal phosphides such as Ni_2P to catalyze nitrate hydrogenation could transform and help us better understand the basic science behind catalytic hydrogenation and, in turn, advance the next generation of oxyanion removal technologies.

INTRODUCTION

Access to clean water is an essential prerequisite for communities to prosper.[1] Unfortunately, higher demand for agricultural products incentivizes the use of ever more land for crop production, limiting the amount of low-lying prairie, riparian forests, and wetlands available for fertilizer biodegradation. Normally, these areas contain minimum oxygen zones that remove some of the toxic contents of agricultural runoff, for example through the anammox biodenitrification process.[2,3,4] Without these, streams, rivers, and groundwater can end up with high concentrations of nitrate—among phosphate and other—ions, which is responsible for birth defects—infant methemoglobinemia or 'blue baby' syndrome[5,6,7,]—and thyroid[8,9,10] and bladder[11,12,13] cancers.[14,15] Downstream, this runoff and urban sewage combine to deliver vast amounts of nitrogen and phosphorus to the sea. In the Gulf of Mexico, this creates one of the largest recurring hypoxic zones in the world—8,776 square miles in 2017—larger than the State of Massachusetts. For these reasons, millions of dollars are spent each year on water purification, and millions more are lost from missed commercial and recreational opportunities.[16]

Removing nitrate (NO_3^-) from water is a difficult task. Under normal, aerobic conditions, NO_3^- is a weakly coordinating, thermodynamically stable, and kinetically persistent form of nitrogen. The water utility of a midsize (pop. 0.5 M) American city in a heavily agricultural region spends *ca.* $1–2 million USD annually to physically remove nitrate.[17] Critically, available physical separation methods—reverse osmosis, ion exchange, and electrodialysis—leave nitrate ions intact, and significant amounts of these are reintroduced into the environment after the process is complete. An alternative chemical degradation method for nitrate removal is hydrogenation.[18,19] Nitrate hydrogenation is a spontaneous energy releasing process ($\Delta G < 0$) by which hydrogen gas (H_2) is used to reduce nitrate to a potentially more useful or benign form of nitrogen, such as ammonia (NH_3) or dinitrogen (N_2), respectively (Scheme 1 and Table 1).

Scheme 1. (a) Catalytic NO_3^- hydrogenation and (b) some of its common intermediates.

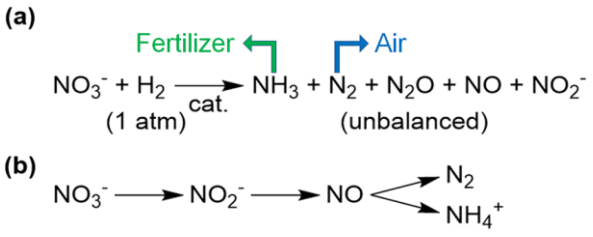

Table 1. Selected nitrate (NO_3^-) hydrogenation reactions under acidic conditions.

Reaction	ΔG^a
$NO_3^- + H_2 + H^+ \rightarrow HNO_2 + H_2O$	-158 kJ/mol
$2NO_3^- + 5H_2 + 2H^+ \rightarrow N_2 + 6H_2O$	-1118 kJ/mol
$NO_3^- + 4H_2 + 2H^+ \rightarrow NH_4^+ + 3H_2O$	-611 kJ/mol

[a]Gibbs free energy change at pH 2.

Unfortunately, nitrate hydrogenation technologies are presently limited by a lack of basic knowledge. Multiple "bimetallic" catalysts for this transformation exist; each consists of a mixture of two metal particles, at least one of which is made of a scarce and expensive noble metal—Ru, Pd, or Pt—which decreases their potential utility and prevents their large-scale deployment.[18,19,20,21,22] A few reports with base metals exist.[23,24,25,26,27] Compounding this problem, some nitrate reduction methods suffer from limited activity and/or poor yields.[18,19] Many they tend to be unselective, often producing nitrite (NO_2^-) or other partially reduced byproducts (NO, N_2O) that are as toxic or more so than nitrate itself (Scheme 1a).[28,18,19] Clearly, new paradigms are needed in order to better understand the basic science behind catalytic nitrate hydrogenation and, in turn, to advance the next generation of nitrate removal technologies.[29,30]

In recent years, binary phosphides (M_xP_y) of the late first row transition metals (M = Mn, Fe, Co, Ni, Cu) emerged as excellent alternatives to noble metal catalysts for the hydrogen evolution reaction (HER).[31,32,33,34,] Chief among these is dinickel phosphide (Ni_2P), whose reconstructed surface structure may mimic the active site of [NiFe] hydrogenase.[35] Initially thought to be a semiconductor, electronic structure calculations revealed that bulk Ni_2P is actually metallic.[36,37,38] Interestingly, their resemblance to noble metals goes well beyond HER, as first row transition metal phosphides are also active catalysts in hydrotreating (HDX, X = S or hydrodesulfurization,[39,40,41,42] O or hydrodeoxygenation[43,44,45], and N or hydrodenitrogenation[46,47]), alkyne hydrogenation,[48,49,50,51] and hydrodearomatization reactions.[52] The ability of Ni_2P and other Earth-abundant, binary metal phosphides to readily and reversibly adsorb hydrogen (H_2), perform a wide range of hydrogenation-like reactions, and achieve high product selectivities strongly suggest that they could also catalyze the hydrogenation of other, typically more challenging reactants, such as nitrate (NO_3^-).

In this paper, we demonstrate that Ni_2P is capable of quickly and completely hydrogenating NO_3^- under near ambient conditions. The reaction is highly selective toward ammonia (NH_3), a potentially reusable form of nitrogen, which becomes protonated under the reaction conditions to ammonium (NH_4^+). Control experiments confirm this is one of the very first low pressure, NO_3^- hydrogenation catalysts based on a non-precious, base metal, whereas the high selectivity for NH_4^+ is distinctive from that of many other conventional noble-metal containing, bimetallic systems.

RESULTS AND DISCUSSION

General observations. Based on our previous work on the phase-selective synthesis of binary nickel phosphides,[36] we prepared Ni_2P nanocrystals from the reaction of nickel(II) acetate with triphenylphosphite in oleylamine and 1-octadecene at 275 °C (Figure 1). Many other earlier and later Ni_2P preparations are available.[31,32,38,40,53,54,55] Without further modification, as made Ni_2P nanocrystals have little catalytic activity. However, annealing under H_2 at 400 °C for 1 h greatly enhances the activity of Ni_2P nanocrystals toward NO_3^- hydrogenation (Figure 2).[31] Structural characterization shows that the bulk of the nanocrystals remains unchanged after H_2 annealing (Figure 1—see Supporting Information or S.I.).[56] Peak widths in the powder X-ray diffraction (XRD) patterns before and after H_2 annealing correspond to a similar Scherrer size of 18 nm (Figure 1). This agrees well with prior studies geared toward catalytic HER and HDX reactions, which showed that the main effect of H_2 annealing on Ni_2P nanocrystals is to remove ligands from their surface (see also removal of adventitious surface species below).[31,57]

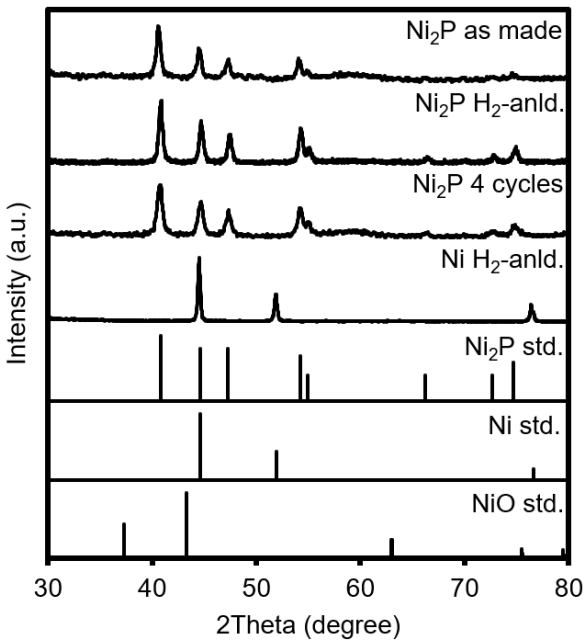

Figure 1. Powder XRD of as made Ni_2P (Scherrer size: 18 nm), H_2-annealed Ni_2P before catalysis (18 nm), recovered Ni_2P after 4 catalytic cycles (14 nm), and H_2-annealed Ni before catalysis (32 nm). Reference patterns shown for comparison (Ni_2P 3–953, Ni 4–850, NiO 47–1049).[56]

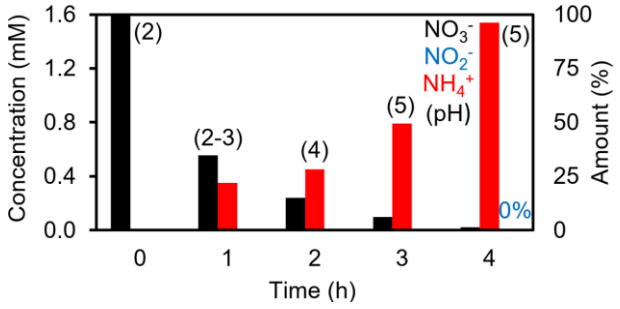

Figure 2. Aqueous nitrate (NO_3^-) hydrogenation over H_2-annealed (activated) Ni_2P nanocrystals (10 mg, 30 mL 1.6 mM $NaNO_3$, initially acidified to pH 2, 1 atm H_2/Ar, 60 °C, see Experimental). (pH values in parenthesis)

Activated Ni_2P catalyzes the ambient (1 atm H_2) hydrogenation of aqueous NO_3^- at 60 °C ("H_2-anld Ni_2P" in Figure 2). When the reaction is started at a relatively low pH such as 2 or 4, it is accompanied by a progressive increase in pH (see below). The reaction is faster under relatively acidic compared to neutral conditions (Figure 3). At pH 2—achieved by acidification with either HCl or H_2SO_4, bubbling

of H_2 through a 1.6 mM solution of NO_3^- in water reduces its concentration to 0.55 mM (66% conversion) within 1 h, and to 0.02 mM (99% conversion) within 4 h. For comparison, 1.6 mM or 22.5 mg/L NO_3^--N is *ca.* twice the maximum level of "nitrogen in nitrate" in drinking water as established by the U.S. Environmental Protection Agency (EPA, ≤ 10 mg/L)[58] and the World Health Organization (WHO, ≤ 11.3 mg/L).[59] At pH 4, NO_3^- is completely reduced within 24 h. At neutral pH, a NO_3^- concentration of 1.3 mM remains (19% conversion) after 24. To our knowledge, there are only a few reports of non-noble metal catalysts for NO_3^- hydrogenation.[23,24] Further, this is one of the first observations of a noble-metal-free hydrogenation catalyst displaying complete (100%) NO_3^- reduction under near ambient conditions.

To gain a deeper insight into the relative activity of Ni_2P, we performed identical NO_3^- hydrogenation experiments in parallel, over Ni_2P *vs.* over conventional bimetallic Pd-Cu/SiO_2 catalysts.[60] By looking at the low conversion data (≤10-20%, at early reaction times), we estimate that the turnover numbers (TON) and frequencies (TOF) achieved with Pd-Cu/SiO_2 are *ca.* 10–25 times higher than those with Ni_2P (see S.I.). However, in terms of reaction rate per gram catalyst (R_g) Pd-Cu/SiO_2 is comparable or only slightly—0–2 times more active—compared to Ni_2P. This implies that Pd-Cu/SiO_2 reduces similar amounts of NO_3^- compared to Ni_2P when using the same mass of catalysts. Considering the cost and, more importantly, the scarcity of precious metals such as Pd, Ni_2P becomes a potentially competitive and perhaps more sustainable substitute to bimetallic catalysts for NO_3^- hydrogenation. In fact, dynamic light scattering (DLS) measurements indicate that the Ni_2P catalyst particles may aggregate somewhat following activation by H_2-annealing. This agglomeration may hinder some of the Ni_2P surface from participating in NO_3^- hydrogenation and may thus reduce catalytic activity. Therefore, we believe that immobilizing the Ni_2P nanocrystals on a high surface area SiO_2 or another suitable support could help in preventing their aggregation and further increasing their activity and durability.

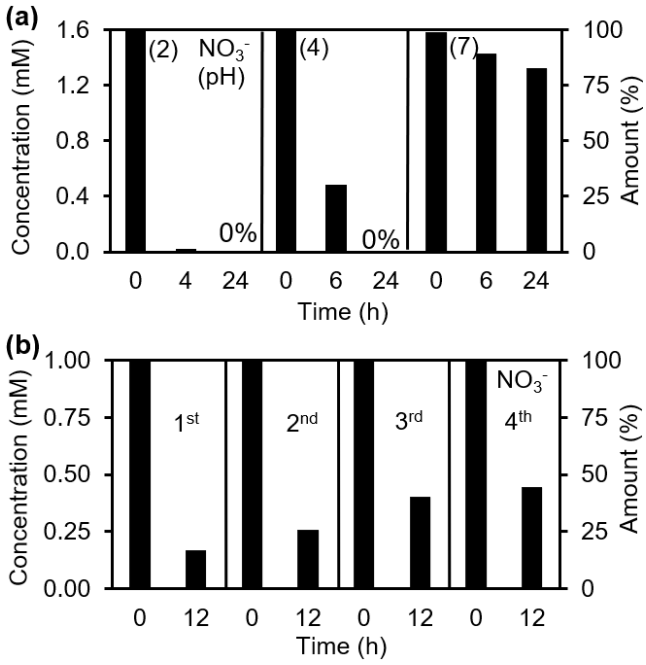

Figure 3. (a) Effect of pH on NO_3^- hydrogenation activity over Ni_2P. (pH values in parenthesis) (b) Consecutive NO_3^- hydrogenation runs over recycled Ni_2P at pH 3 (10 mg, 30 mL 1 mM $NaNO_3$, 1 atm H_2/Ar, 60 °C, see Experimental).

Unique selectivity for NH_3. Analysis of the aqueous solution after catalysis reveals that the majority (95%) product of NO_3^- hydrogenation over Ni_2P is NH_4^+, with no nitrite (NO_2^-) being detected. In contrast, conventional bimetallic catalysts (*e.g.*, Pd-Cu/SiO_2) often yield mixtures of products,[19] with NO_2^- being the only major product in the absence of the noble metal. Uniquely selective catalysts like Ni_2P, which are capable of producing a single NO_3^- hydrogenation product such as N_2 or NH_3 are highly desirable from a practical perspective. When the only product is dinitrogen (N_2), this can simply be released to the atmosphere without causing further harm to the environment. In the rarer—under 1% of catalysts reported to date, see S.I.—but still very valuable case when the only product is ammonia (NH_3 or NH_4^+), this could potentially be recycled and reused as fertilizer, for example through available NH_4^+ separation techniques.[61,62,63,64,65] The economic benefit of the latter is highlighted by the fact that every year, ~17 million tons of ammonia- and urea-based fertilizers are used in the US alone.[66] A large fraction of these are produced by the energy-intensive Haber–Bosch process which, unlike the system reported here, requires very high temperatures and pressures to operate.[67]

The observed effect of pH on activity suggests a dependence of the reaction kinetics on the concentration of protons.[68] This can be explained by looking at the overall chemical equation required to hydrogenate nitrate to ammonium, which utilizes two protons to be fully balanced (Table 1). Of these, one H^+ equivalent is needed for each NO_3^- ion

that is reduced—the redox reaction *per se*—while, under the conditions studied here (2 ≤ pH ≤ 7, see above), a second H^+ equivalent is needed to protonate each NH_3 molecule produced, to its conjugate acid, NH_4^+ (pK_a = 9.3).

Catalytic control experiments. To test the true catalytic nature of the Ni_2P nanocrystals, we conducted the following experiments: First, attempts at achieving NO_3^- hydrogenation in the absence of Ni_2P were unsuccessful, with null activity or conversion detected after several hours (see S.I.). Second, repeating the reaction with activated Ni_2P but without the flow of H_2 resulted in small but measurable catalytic activity (43% conversion after 12 h). We attribute this residual activity to the presence of hydrogen atoms (H·) adsorbed onto the activated Ni_2P surface, arising from dissociation of H_2 during the annealing step. Once these residual surface-H reactive sites are completely consumed, Ni_2P is no longer active or recyclable unless a continuous flow of H_2 is supplied. In the presence of Ni_2P and H_2 flow, we observe single cycle TON and TOF numbers of up to *ca.* 24 and 6/h, respectively (see S.I.).

In addition to control experiments, we also tested the recyclability of Ni_2P. Because of the aforementioned increase in pH during hydrogenation, we first sought a way to maintain a relatively low, acidic pH during recycling. However, even relatively inert buffers such as piperazine-N,N′-bis(2-ethanesulfonic acid) (PIPES) or 2-(*N*-morpholino)ethanesulfonic acid (MES) failed to maintain the desired pH.[69] This strongly indicates that, like nitrate, these otherwise noncoordinating alkylsulfonate buffers may be reacting with Ni_2P under our NO_3^- hydrogenation conditions. Fortunately, we were able to solve this problem and maintain a pH of *ca.* 3 throughout our catalytic reactions by continuously adding a concentrated stock solution of acid (see Experimental). In this way, Ni_2P maintains high activity for at least 4 cycles under the flow of H_2, augmenting the overall TON to 45 (Figure 3b & S.I.). A slow decrease in conversion after multiple cycles may be attributed to slow repassivation of the catalyst surface and/or to partial catalyst etching. Peak widths observed by powder X-ray diffraction (XRD) after 4 catalytic cycles correspond to a Scherrer size of 14 nm, slightly smaller than the 18 nm measured after annealing and before catalysis. Efforts to further improve catalyst stability while maintaining activity, for example by immobilization in a porous support and reannealing under H_2, respectively, are ongoing. Together, these control experiments clearly establish that H_2 flow and substoichiometric amounts of Ni_2P are requisites for sustained NO_3^- hydrogenation, affirming that Ni_2P is a catalyst for this reaction.

Probing intermediates. In contrast to NO_3^- hydrogenation over the relatively well studied bimetallic catalysts (see above),[22,70,71] little is known about the mechanism of NO_3^- hydrogenation over Ni_2P. Because nitrite (NO_2^-) and nitric oxide (NO) are known intermediates in Pd- and Ru-based bimetallic NO_3^- hydrogenation, we tested both of these reactants here. Indeed, as is the case for NO_3^-, aqueous NO_2^- is quickly and completely hydrogenated in the presence of Ni_2P under a flow of H_2 (Figure 4a). This is significantly higher than the ~25% NO_2^- conversion observed with a zerovalent Ni foam at room temperature.[72] Compared to NO_3^- hydrogenation, NO_2^- hydrogenation over Ni_2P is a little faster, even at neutral pH. Interestingly, the reaction selectivity is also different, producing much smaller amounts of NH_4^+ (Figure 4a). Because no other soluble nitrogen species is detected, we strongly suspected that the remainder nitrogen balance must be gaseous products. To test this hypothesis, we repeated the hydrogenation reaction using ^{15}N-labeled Na^*NO_2 (98%), and easily identified the evolution of singly- and doubly-labeled $^{*(*)}N_2$ ($^{15}N^{14}N$ and $^{15}N^{15}N$), along with some $^*NO$ (^{15}NO) using GC-MS (m/z=29, 30, and 31, respectively) (see S.I.).

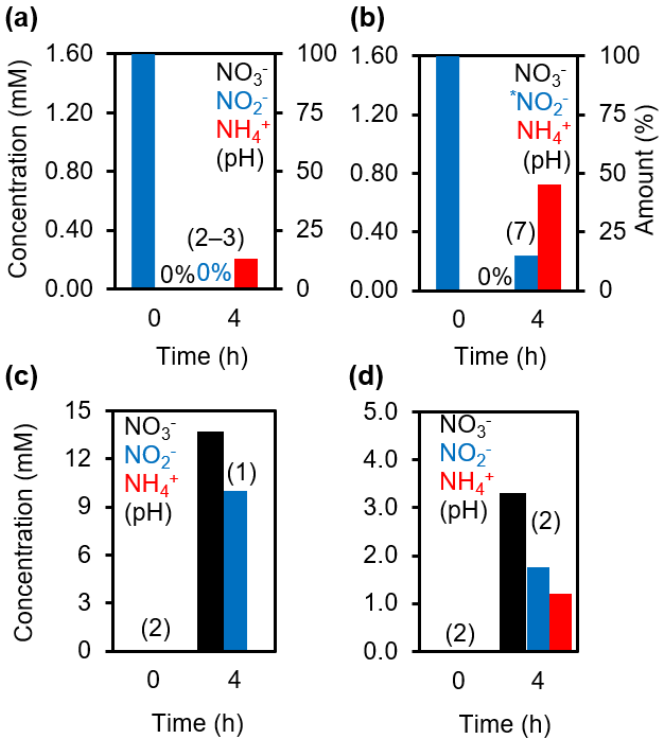

Figure 4. (a) Nitrite (NO_2^-) hydrogenation over Ni_2P (10 mg, 30 mL 1.6 mM $NaNO_2$, initially acidified to pH 2, 1 atm H_2/Ar, 60 °C). (b) $^{15}NO_2^-$ hydrogenation over Ni_2P (10 mg, 30 mL 1.6 mM $Na^{15}NO_2$, initially acidified to pH 2, 1 atm H_2/Ar, 60 °C, batch reaction). Nitric oxide (NO) hydrogenation in the absence (c) and presence (d) of Ni_2P (30 mL deionized water, 1 atm NO/H_2, 60 °C) (see Experimental). (pH values in parenthesis)

The change in product selectivity from NH_4^+ to N_2 when switching the initial hydrogenation reactant from NO_3^- to NO_2^- has important practical implications. Forming N_2 requires an entropically difficult, bimolecular step where two reactive N-species must come together on the catalyst surface. Prior work on bimetallic catalysts has indicated that higher concentrations of NO_2^- intermediate increase the selectivity for N_2.[73,74] In our experiments above, the effective concentration of NO_2^- is obviously much higher during NO_2^- hydrogenation than during NO_3^- hydrogenation, which helps explains the observed selectivity. Critically, the small, steady state concentration of NO_2^- intermediate during NO_3^-

hydrogenation must depend on the active surface, and must thus be susceptible of tuning through catalyst modification.

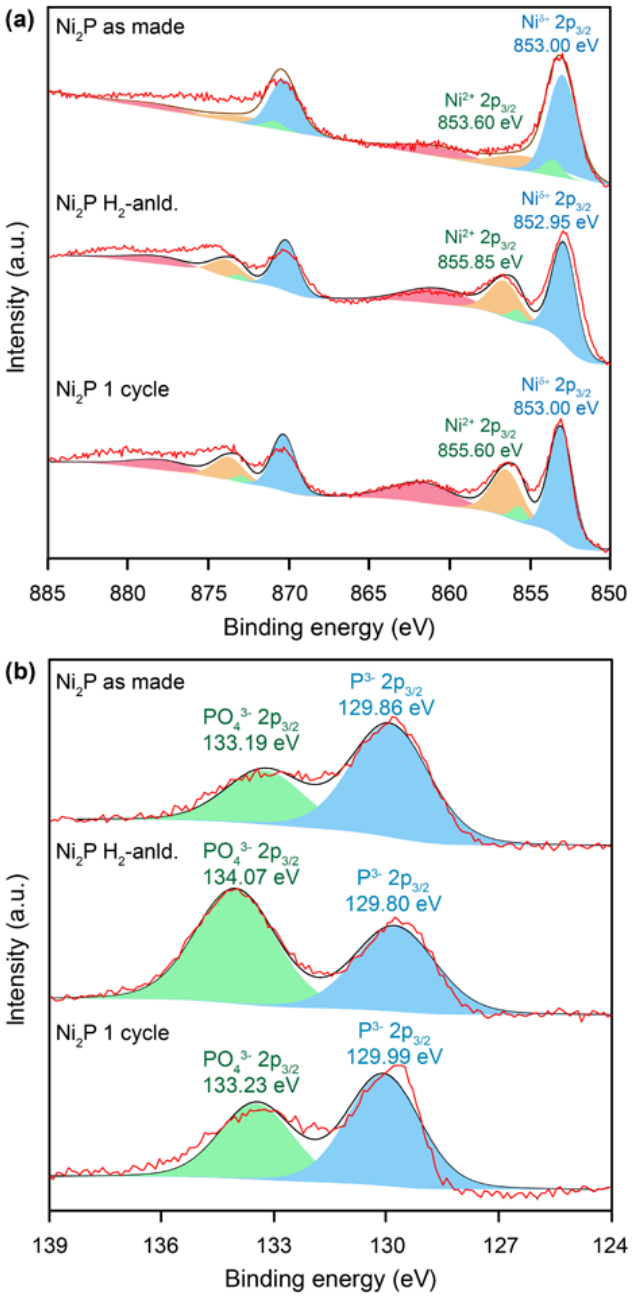

Figure 5. XPS of as made, H_2-annealed (activated), and recycled (after 1 cycle) Ni_2P nanocrystals showing the Ni $2p_{3/2}$ (a) and P 2p (b) regions.

Similar to NO_3^- and NO_2^-, NO is also hydrogenated in the presence of Ni_2P. However, this reaction is more complicated and less selective compared to the former two, in part because even in the absence of catalyst, NO can disproportionate—into NO_x^- and NH_4^+ products—and/or become oxidized—to NO_x^-—by leftover O_2 in aqueous solution (Figure 4c, d).[75,76] Based on our results, we conclude that both NO_2^- and NO are competent intermediates in NO_3^- hydrogenation over Ni_2P (Scheme 1b).

Surface chemistry and cocatalyst effects. Because catalytic activity depends on surface chemistry, we measured and compared the X-ray photoelectron spectroscopy (XPS) of Ni_2P at different stages of synthesis, activation, and catalysis. As made, H_2-annealed, and post-catalysis ("1 cycle") Ni_2P each show signals corresponding to two main Ni and two main P species (Figure 5). In all samples, the Ni $2p_{3/2}$ region shows a main peak at a binding energy of 853.0 eV—slightly higher than that of Ni^0 (852.6 eV)—which is consistent with previous reports for the very small positive charge ($Ni^{\delta+}$) in Ni_2P (Table 2).[53,56] Another smaller peak—at 853.6 eV for as made Ni_2P, and at 855.7 eV for H_2-annealed and 1 cycle Ni_2P (post-catalysis)—corresponds to oxidized Ni^{2+}; interestingly, the former is normally associated with NiO, while the latter is with $Ni(OH)_2$.[77,78] In all samples, the P 2p region also exhibits two peaks, a main one at 129.1 eV corresponding to phosphide (P^{3-}) in Ni_2P, and another smaller peak at 133.2 eV characteristic of a fully oxidized phosphorous species (P^{5+}), most likely PO_4^{3-}.[53,56]

Table 2. Selected XPS measurements of Ni_2P nanocrystals used in catalytic nitrate (NO_3^-) hydrogenation.[a]

Assignment, energy (eV)	As made Ni_2P	H_2-anld. Ni_2P	Ni_2P 1 cycle
$Ni^{\delta+}$ $2p_{3/2}$ 853.0(1)	40%	34%	32%
Ni^{2+} (NiO) $2p_{3/2}$ 853.6(1)	4%	na	na
Ni^{2+} ($Ni(OH)_2$) $2p_{3/2}$ 855.7(1)	na	3%	3%
P^{3-} $2p_{3/2}$[b] 129.1(4)	68%	57%	63%
P^{5+} $2p_{3/2}$[b] 133.2(7)	32%	43%	37%

[a]Calibrated using C 1s peak at 284.6 eV as reference. Assignments agree with NIST XPS database[77] as well as with previous reports.[53,56] [b]P $2p_{3/2}$ - P $2p_{1/2}$ spin-orbit splitting Δ=0.87 eV, P $2p_{3/2}$ overlaps P $2p_{1/2}$.

Interestingly, both of the relative amounts of oxidized Ni (Ni^{2+}) and P (PO_4^{3-}) species on the Ni_2P surface increase after annealing, and remain similarly high after catalysis (Table 2). We explain these observations as follows: After initial synthesis, as made Ni_2P nanocrystals contain small amounts of an NiO impurity on their surface.[79] During activation, H_2 annealing removes this NiO impurity, specifically by reducing it to a small, relatively amorphous—XRD silent—amount of zerovalent (metallic) Ni^0, or more $Ni^{\delta+}$. However, these latter species—surface Ni^0 or $Ni^{\delta+}$—are relatively reactive, and quickly transform into $Ni(OH)_2$ upon exposure to air before XPS measurements are made. Similarly, some $Ni(OH)_2$ and PO_4^{3-} species may form by exposure of surface sites upon removal of surface passivating ligands during H_2 annealing.[31,57] Annealing makes the Ni_2P surface

much more reactive, and also more susceptible to oxidation—by air or moisture—during handling and characterization.

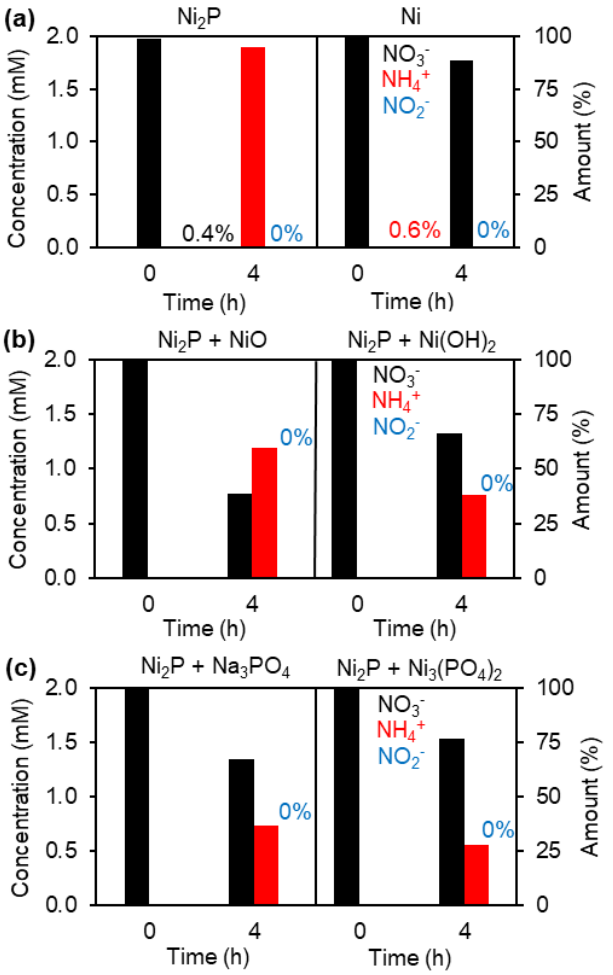

Figure 6. NO_3^- hydrogenation over Ni_2P *vs.* Ni (a). NO_3^- hydrogenation over Ni_2P with equimolar amounts of Ni(II) (b), PO_4^{3-} and both sources added (c) (10 mg, 30 mL 2 mM $NaNO_2$, initially acidified to pH 2, 1 atm H_2/Ar, 60 °C, see Experimental).

To test whether the observed Ni^{2+} and PO_4^{3-} species contribute—either separately or together—to NO_3^- hydrogenation, we repeated our catalytic experiments in the presence of sources of Ni^{2+} or PO_4^{3-} or both ions, in addition to Ni_2P (Figure 6). Compared to the Ni_2P only-catalyzed reaction, adding NiO decreased NO_3^- hydrogenation activity by 35%, while adding $Ni(OH)_2$ decreased it by 62%. In turn, adding Na_3PO_4 decreased NO_3^- hydrogenation activity by 63%, while adding $Ni_3(PO_4)_2$ decreased it by 71%. Because either or both Ni(II) and P(V) sources added on purpose clearly hinder and reduce catalytic activity, we conclude that these impurities, which are observed by XPS, do not contribute or act as cocatalysts in NO_3^- hydrogenation.

Finally, we probed whether a small amount of undetected Ni^0 could be responsible for the NO_3^- hydrogenation results shown here. To do this, we compared the activity and selectivity of nanocrystalline Ni_2P with that of Ni made independently, after each of them was annealed and activated in the same way under H_2 (see Experimental). At 1 atm H_2 and 60 °C for 4 h, a 2 mM solution of NO_3^- is almost completely hydrogenated, down to 0.02 mM (99% conversion) over Ni_2P, with a very high selectivity for NH_4^+ (96%) (Figure 6a). In contrast, under identical reaction conditions, the same solution is only slightly hydrogenated, down to 1.7 mM NO_3^- (17% conversion) over Ni, without producing any measurable NH_4^+. It is known that Ni reacts with HNO_3 to give gaseous nitrogen oxides such as nitric oxide (NO).[23,80] Because Ni is much less reactive, and because it has a very different selectivity toward NO_3^- hydrogenation compared to Ni_2P, we conclude that any traces of metallic (zerovalent) Ni, if present, cannot be responsible for the reactivity observed with Ni_2P.

Insights from computations: gas *vs.* liquid phase. Using DFT (VASP, PBE, see Experimental) we calculated the change of energy ΔE for NO_3^- hydrogenation in the gas phase (Table 3). Each individual reaction step is highly exothermic. Using VASPsol to account for electrostatics, cavitation, and dispersion between solute and solvent, we also calculated ΔE for NO_3^- hydrogenation in the liquid phase (Table 3). These results strongly indicate that the individual NO_2^- hydrogenation step becomes is least exothermic and, in the absence of appropriate conditions, somewhat more difficult. It is possible to combine NO_2^- and NO^- hydrogenations into a single step (last entry, Table 3) but, because this requires breaking two H_2 bonds, it may be kinetically difficult. Therefore, these calculations point to nitrite (NO_2^-) being the most likely bottleneck step in nitrate (NO_3^-) hydrogenation in the absence of a suitable catalyst.

Table 3. Calculated energy changes for different steps of nitrate (NO_3^-) hydrogenation.

Reaction	ΔE_g[a] (eV)	ΔE_l[b] (eV)
$NO_3^- + H_2 \rightarrow NO_2^- + H_2O$	-1.12	-1.57
$NO_2^- + H_2 \rightarrow NO^- + H_2O$	-0.41	-0.22
$NO^- + H_2 \rightarrow H_2NO^-$	-0.68	-0.98
$H_2NO^- + H_2 \rightarrow NH_2^- + H_2O$	-1.50	-1.95
$NO_2^- + 2H_2 \rightarrow H_2NO^- + H_2O$	-1.05	-1.20

[a]Gas phase energy change. [b]Liquid phase energy change.

Ni_2P(001) surface reconstruction. The PBE calculated surface lattice constants (*a*) of Ni_2P(001) and fcc Ni(111) are 5.872 Å and 2.488 Å, respectively. Thus, the surface unit cell of Ni_2P(001) is *ca.* 5.6 times larger than that of Ni(111). Along the (001) direction, the Ni_2P unit cell has a bilayer structure, with three Ni and two P atoms in one plane, and three Ni and one P atom in the other. Cutting a Ni_2P crystal along the (001) direction thus generates two types of surface terminations: a Ni-rich or "Ni_3P" surface (Figure 7a), and a P-rich or "Ni_3P_2" surface (Figure 7b). Using DFT, we determine that a large variety of adsorbates (H, O, N, NO) induce a reconstruction of the Ni-rich surface (Figure 7c). This reconstruction involves the surface layer as well as atoms deeper in the structure. First, the three Ni atoms surrounding one of the P atoms on the second layer move

closer to each other, allowing the second P atom on the second layer to move up to the top layer. Thus, the top layer has a similar chemical composition to the P-rich termination, but rotated by 30°. The P atoms directly beneath the one that has already moved also move up. In total, almost half of the P atoms move up. When the thickness of the slab is larger than 3 bilayers, this restructuring remains stable after removal of the adsorbate. In vacuum, the reconstructed surface is about 0.09 eV more stable than the unreconstructed structure and, in solution, it is about 0.05 eV more stable. We also note that the clean Ni-rich termination, although unstable towards reconstruction, is metastable. DFT calculations show that H atoms only induce reconstruction locally.

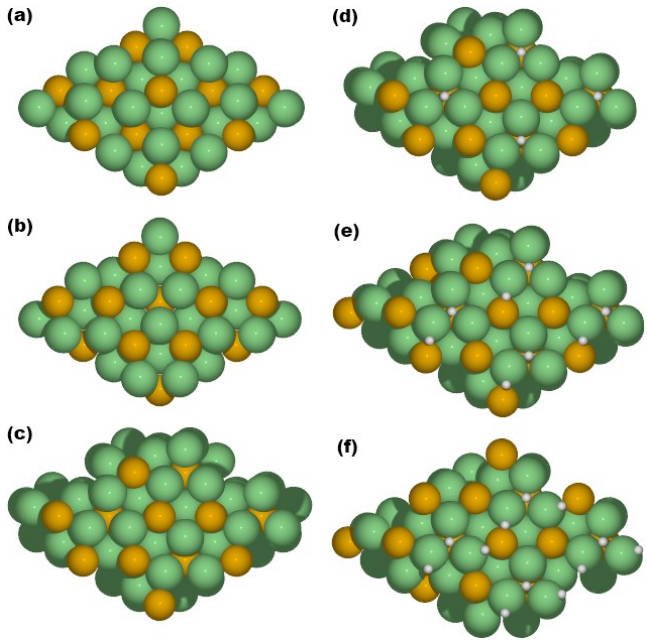

Figure 7. (a-c) Different terminations of the $Ni_2P(001)$ surface: (a) Ni-rich or "Ni_3P" surface, (b) P-rich or "Ni_3P_2" surface, and (c) reconstructed Ni-rich surface. The three Ni atoms in each P-rich surface unit cell are close to each other, forming a local configuration resembling that of the Ni(111) surface, while the Ni atoms in the Ni-rich surface unit cell are more open. (d-f) Top view of H adsorption on Ni_2P surfaces: (d) 1 H, (e) 2 H, (f) 3 H per unit cell (see Table 4). Ni: green; P: gold; H: (small) white.

Hydrogen adsorption. Figure 7d-f, Table 4, and Figure 8 show DFT calculations for the hydrogen adsorption on the Ni-rich terminated surface. Because of the aforementioned reconstruction, the results are similar to that with P-rich termination. On the Ni-rich surface, the adsorption energies per H atom with a vacuum interface are -0.60 eV, -0.27 eV and -0.15 eV with 1, 2, and 3 H atoms in a single unit cell, respectively. This corresponds to -0.70 eV, -0.35 eV, and -0.17 eV, respectively, for the P-rich surface. At low coverage on the P-rich surface, with 1 H adatom in each unit cell, the adsorption energy is about -0.70 eV, but with 2 or 3 H adatoms in each unit cell, adsorption becomes much weaker. In other words, in the presence of H_2 (gas), increasing the hydrogen coverage above 1 H per unit cell does not decrease the total energy. Thus, the calculated hydrogen saturation coverage on $Ni_2P(001)$ is about 1 H per unit cell, or *ca.* 3 nm^{-2}. This is in sharp contrast to what is observed for either Pd(111) and Ni(111), where there are very weak interactions between H adatoms separated $\sqrt{3}$ or more lattice constants. In these cases, and without even considering subsurface adsorption, the hydrogen saturation coverage is *ca.* 15-18 nm^{-2}.

Table 4. Select adsorption energies (eV) on different metal surfaces.

	Ni_2P (001)		Ni (111)	Pd (111)	Reference
	Water	Vacuum	Vacuum	Vacuum	
1 H[a]	-0.72	-0.70	-0.59 (r7×r7)	-0.63 (r7×r7)	H_2(g)
2 H[a]	-0.36	-0.35	-0.59 (2×2)	-0.62 (2×2)	
3 H[a]	-0.18	-0.17	-0.58 (r3×r3)	-0.62 (r3×r3)	
NO_3	-2.40	-2.51	-2.24 (2×2)	-1.78 (2×2)	NO_3(g)
NO_2	-2.17	-2.57	-1.97 (2×2)	-1.64 (2×2)	NO_2(g)
NO	-2.32	-2.33	-2.48 (2×2)	-2.30 (2×2)	NO(g)

[a]Number of H per Ni_2P unit cell area. Unit cells for fcc(111) metal calculations (with 1 H per unit cell) are chosen to roughly cover the same regime of H coverage (per unit area) as on Ni_2P.

Our results agree with prior computational studies, which found that the total adsorption energy is similar when the coverage is doubled (or tripled) on $Ni_2P(001)$, but roughly doubles (triples) for Pd(111) and Ni(111) for the selected coverage range (using a larger supercell).[35] The same study explained the enhanced activity of Ni_2P toward HER based on a smaller barrier for recombination and desorption of H_2 on Ni_2P relative to Pd and Ni.

Unlike the case for H, the calculated adsorption energies of nitrogen-based oxyanions, encased explicitly within water clusters and with their charge balanced by H_3O^+ do not show significant differences across the three different metal surfaces (see S.I.). In Table 4, we listed the adsorption energies of an initially neutral NO_x molecule on various surfaces, which show similar behavior. Therefore, a new possible explanation for the enhanced hydrogenation ability of Ni_2P observed here is that, because its hydrogen (H) saturation coverage is much lower than that of other metals, Ni_2P retains enough surface sites available for coadsorption of NO_x.

. In contrast, the surface of pure Pd and Ni is almost completely covered by H, and the adsorption of NO_3^- is especially difficult.

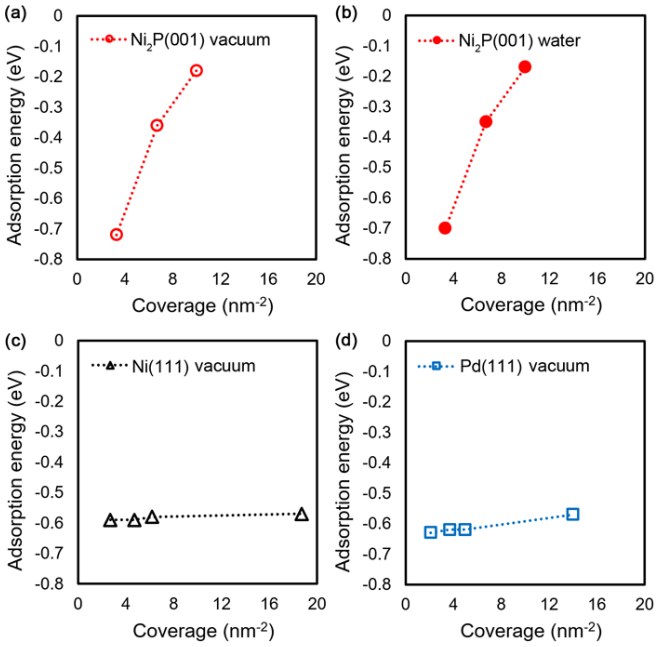

Figure 8. Adsorption energy as a function of H coverage for (a) $Ni_2P(001)$ in vacuum, (b) $Ni_2P(001)$ in water, and (c) Ni(111) and (d) Pd(111) in vacuum.

CONCLUSIONS

In summary, nitrate is quickly hydrogenated under relatively mild conditions (1 atm H_2, 60 °C, acidic pH) in the presence of activated Ni_2P nanocrystals. The reaction produces ammonia (NH_3) with very high selectivity (96%), a relatively rare feature shared by only a sliver of known nitrate hydrogenation catalysts. This is also one of the first observations of nitrate hydrogenation with a non-noble-metal catalyst, and its high selectivity toward ammonia allows to envision a process by which nitrate, a pollutant, could be recycled back to more useful fertilizer.

Unlike bimetallic catalysts, single phase Ni_2P is capable of completely reducing nitrate beyond the nitrite (NO_2^-) stage. This is confirmed by separate experiments where nitrite hydrogenation was used as reactant. Interestingly, the selectivity changed from mostly NH_3 for nitrate hydrogenation, to a mixture of NH_3 and N_2—plus some NO—for nitrite hydrogenation. Because product selectivity is linked to the local concentration of nitrite on the catalyst surface, we believe other metal phosphide nanophases may enable to purposely tune the hydrogenation selectivity toward N_2.

Usually inert alkylsulfonate buffers react with Ni_2P under hydrogenation conditions, suggesting that other tough hydrogenation reactants, including polluting oxyanions and oxysalts (ClO_x^{n-}, SO_n^{2-}, etc.) could also be chemically removed by Ni_2P-mediated hydrogenation. A self-sustaining, hydrogen-free photocatalytic nitrate reduction in the absence of sacrificial agents may also be envisioned. Neither Ni(II) nor P(V) species, which are observed by XPS appear to have an effect on nitrate hydrogenation. Nor does zerovalent Ni, which may be present as a small amorphous impurity after activation by H_2 annealing. A small yet measurable decrease in activity after 4 consecutive cycles, perhaps due to partial etching or re-passivation (fouling) of the Ni_2P surface, may be preventable by either immobilization on a support, or by reactivation (H_2- reannealing), respectively.

The $Ni_2P(001)$ surface has a smaller density of surface Ni atoms than the Ni(111) surface. DFT shows that the reconstructed Ni-rich and P-rich surfaces display ensembles of Ni atoms that locally resemble the Ni(111) surface. The unreconstructed Ni_2P surface, having unfavorable H adsorption may be inactive. However, treatment with H_2 and other adsorbates results in reconstruction and activation. Alternatively, because $Ni_2P(001)$ has an H saturation density that is about $^1/_5$ to $^1/_6$ smaller than that of Ni(111) and Pd(111), the former may be able to better accommodate the binding of otherwise very weakly coordinating nitrate ions, while the latter two may not. In addition to advancing the scope of important hydrogenations catalyzed by Earth abundant transition metal phosphides, this work will help in improving our understanding the basic science behind catalytic nitrate hydrogenation and, in turn, advancing the next generation of technologies for the safe and effective removal of nitrate from water.

EXPERIMENTAL

Materials. Triphenylphosphite ($P(OPh)_3$, 97%) and nickel(II) acetylacetonate hydrate ($Ni(acac)_2{\cdot}H_2O$) were purchased from Strem; nickel(II) acetate tetrahydrate ($Ni(OAc)_2{\cdot}4H_2O$, ≥99.0%), mesoporous silica (SiO_2, SBA-15), oleylamine (technical grade, 70%), 1-octadecene (ODE, technical grade, 90%), and sodium nitrite ($NaNO_2$, 99.999%) from Sigma; palladium chloride ($PdCl_2$) from D. F. Goldsmith; copper nitrate ($Cu(NO_3)_2$, 99%), sulfuric acid (H_2SO_4, certified ACS plus), hydrochloric acid (HCl, certified ACS plus), sodium nitrate ($NaNO_3$, certified ACS), acetone, and toluene (99.9%) from Fisher; hydrogen gas (H_2) and argon gas (Ar) from Airgas; nitric oxide (NO, 99%) from Praxair; $Na^{15}NO_2$ (98% ^{15}N-labeled) is from Cambridge Isotope Laboratories. Colorimetric kits (0.10-25.0 mg/L NO_3-N; 0.002-1.00 mg/L NO_2-N; 2.0-150 mg/L NH_4-N) were purchased from Merck. All chemicals were used as received. MillQ water is used all over the experiments

Synthesis. *Ni_2P.* $Ni(OAc)_2{\cdot}4H_2O$ (0.36 mmol, 90 mg), oleyl amineNH_2 (5 mmol, 1.35g, 1.66 mL), and ODE (5 g, 6.34 mL) were degassed under a vacuum at 80 °C for 1 h, refilled with Ar, then heated to 275 °C. The mixture was heated to 275 °C, 0.55 mL of $P(OPh)_3$ were injected, the temperature maintained while stirring for 30 min. The mixture was cooled to room temperature (21 °C, R.T.), and solids were isolated and washed twice with toluene by centrifugation at 4500 rpm for 3 min. *Ni.*[81] $Ni(acac)_2$ (7.8 mmol, 2 g) and oleyl amine (78 mmol, 20.8 g, 25.6 mL) were degassed under dynamic vacuum at 100 °C for 1 h. The mixture was refilled with dry Ar and heated to 220 °C for 2 h. After cooling to R.T., 40 mL acetone were added. Solids were isolated by centrifugation at 4500 rpm for 5 min. *Pd-Cu/SiO_2.*[60] An aqueous solution of $PdCl_2$ (0.113 M, 0.44 mL) was added to SBA-15 (0.1 g) and the mixture let dry at 100 °C for 12 h. A solution of $Cu(NO_3)_2$ (0.166 M, 0.056 mL) was then added, and the mixture let dry at 100 °C for 12 h. *H_2 Annealing.* Ni_2P or

Ni were dried under dynamic vauum for 15 min, then annealed at 400 °C for 1 h under a flow of H_2/Ar (1 atm). Pd-Cu/SiO_2 was annealed at 450 °C for 2 h under a flow of H_2/Ar.

Characterization. UV-Vis absorption spectra were collected with a photodiode-array Agilent 8453 UV-Vis Spectrometer. Powder X-ray diffraction (XRD) was recorded using a Rigaku Ultima IV diffractometer with a Cu Kα radiation (40 kV, 44 mA). X-ray photoelectron spectroscopy (XPS) was performed using a Kratos Amicus/ESCA 3400 instrument. The sample was irradiated with 240 W unmonochromated Mg Kα X-rays, and photoelectrons emitted at 0° from the surface were energy analyzed using a DuPont type analyzer. The pass energy was set at 150 eV. CasaXPS was used to process raw data files. The binding energy of C 1s at 284.6 eV was used as reference. Transmission electron microscopy imaging was performed on an FEI Tecnai G2-F20 scanning transmission electron microscope. Gas chromatography-mass spectroscopy was acquired on an Agilent 7250 GC Q-TOF. Dynamic light scattering (DLS) was performed on a Malvern Zetasizer Nano ZS.

Catalytic Hydrogenation. 10 mg dry catalyst were placed in a 3-neck round bottom flask. A solution of $NaNO_3$ or $NaNO_2$ in deionized water (30 mL), previously sparged with Ar for 15–20 min, and with a pH adjusted by the addition of either HCl or H_2SO_4, was added. A 5-10% mixture of H_2 in Ar was flowed at a rate of *ca.* 5 mL/min while vigorously stirring at a rate of (700-1200 rpm) and a temperature at 60 °C. When $Na^{15}NO_2$ was used, the reaction was simply filled with H_2/Ar and run in batch (closed) to facilitate analysis of the headspace (100 μL) by GC analysis. When NO was used, a NO:H_2 mixture was used. *pH control and recyclability.* To maintain a constant acidic pH, a solution of either HCl or H_2SO_4 was continuously added to the mixture *via* syringe pump. Similarly, to start a new cycle, a small aliquot of a concentrated $NaNO_3$ solution was re-introduced. *NO_3^-, NO_2^- and NH_4^+ Quantification.* Colorimetry methods were used to determine the aqueous concentrations of NO_3^-, NO_2^- and NH_4^+.

Calculations. Density functional Theory (DFT) calculations of the total energies were performed using the VASP package (v5.4)[82,83] with the standard PAW potentials[84,85] and the PBE functional.[86] The energy cutoff of the plane-wave basis sets is 400 eV. The bulk Ni_2P crystal is hexagonal (space group $P\bar{6}2m$, No. 189), with 6 Ni and 3 P atoms in each supercell. The theoretical lattice constants obtained from energy minimization are $a = b = 5.872$ Å, and $c = 3.369$ Å. The $Ni_2P(001)$ surface was modeled by periodic arrays of slabs separated by 12 Å of vacuum. Reactants were adsorbed on one side (the top) of the slab. Both adsorbates and the substrate atoms are allowed to relax, with the exception of the bottom layer of atoms which were fixed at their bulk positions. The Brillouin zone was sampled using a (12×12×1) grid. All energetics reported were average values of results using 4 to 7 bilayers of substrates. Most of the calculations were performed with the standard VASP code that is most applicable to gas-solid interface. Some calculations were also performed using VASPsol[87] which includes the effect of electrostatics, cavitation, and dispersion between a solute and solvent.

ASSOCIATED CONTENT

Supporting Information. Additional structural characterization, catalysis and conversion data, control experiments, and computational details are shown in the Supporting Information. This material is available free of charge *via* the Internet at http://pubs.acs.org

AUTHOR INFORMATION

Corresponding Author

*vela@iastate.edu

ACKNOWLEDGMENT

J.V. thanks the U.S. National Science Foundation for a grant from the Division of Chemistry, Macromolecular, Supramolecular, and Nanochemistry Program (1905066). D.J.L. and J.W.E. were supported for the theoretical analysis in this paper by the U.S. Department of Energy (USDOE), Office of Basic Energy Sciences, Division of Chemical Sciences, Geosciences, and Biosciences through the Ames Laboratory Chemical Physics program. Ames Laboratory is operated for the USDOE by Iowa State University under Contract No. DE-AC02-07CH11358. D.J.L. also acknowledges use of computational resources from NERSC. XPS work was performed at the Materials Analysis and Research Laboratory of the ISU Office of Biotechnology. We thank Dapeng Jing for assistance. J.V. and J.W.E. thank the Iowa State University Office of the Vice President for Research for PIRS funds facilitating collaborative research.

REFERENCES

(1) Brookes, J. D.; Carey, C. C. Goal 6—Rising to the Challenge: Enabling Access to Clean and Safe Water Globally. *UN Chronicle* **2015**, *LI*(4).

(2) Lan, P.; Kuypers, M. M. M. Microbial Nitrogen Cycling Processes in Oxygen Minimum Zones. *Annu. Rev. Mar. Sci.* **2011**, *3*, 317–345.

(3) Van Hulle, S. W. H.; Vandeweyer, H. J. P.; Meesschaert, B. D.; Vanrolleghem, P. A.; Dejans, P.; Dumoulin, A. Engineering Aspects and Practical Application of Autotrophic Nitrogen Removal from Nitrogen Rich Streams. *Chem. Eng. J.* **2010**, *162*, 1–20.

(4) Fowler, D.; Coyle, M.; Skiba, U.; Sutton, M. A.; Cape, J. N.; Reis, S.; Sheppard, L. J.; Jenkins, A.; Grizzetti, B.; Galloway, J. N.; Vitousek, P.; Leach, A.; Bouwman, A. F.; Butterbach-Bahl, K.; Dentener, F.; Stevenson, D.; Amann, M.; Voss, M. The Global Nitrogen Cycle in the Twenty-First Century. *Phil. Trans. Royal Soc. B* **2013**, *368*, 20130164.

(5) Brender, J. D.; Weyer, P. J.; Romitti, P. A.; Mohanty, B. P.; Shinde, M. U.; Vuong, A. M.; Sharkey, J. R.; Dwivedi, D.; Horel, S. A.; Kantamneni, J.; Huber, J. C. Jr. Zheng, Q. Werler, M. M.; Kelley, K. E.; Griesenbeck, J. S.; Zhan, F. B.; Langlois, P. H.; Suarez, L.; Canfield, M. A. Prenatal Nitrate Intake from Drinking Water and Selected Birth Defects in Offspring of Participants in the National Birth Defects Prevention Study. *Environ. Health Perspect.* **2013**, *121*, 1083–1089.

(6) Manassaram, D. M.; Backer, L. C.; Moll, D. M. A Review of Nitrates in Drinking Water: Maternal Exposure and Adverse Reproductive and Developmental Outcomes. *Environ. Health Perspect*. **2006**, *114*, 320–327.

(7) Knobeloch, L.; Salna, B.; Hogan, A.; Postle, J.; Anderson, H. Blue Babies and Nitrate-Contaminated Well Water. *Environ. Health Persp.* **2000**, *108*, 675–678.

(8) Kilfoy, B. A.; Zhang, Y.; Park, Y.; Holford, T. R.; Schatzkin, A.; Hollenbeck, A.; Ward, M. H. Dietary Nitrate and Nitrite and the Risk of Thyroid Cancer in the NIH-AARP Diet and Health Study. *Int. J. Cancer* **2011**, *129*, 160–172.

(9) Ward, M. H.; Kilfoy, B. A.; Weyer, P. J.; Anderson, K. E.; Folsom. A. R.; Cerhan, J. R. Nitrate Intake and the Risk of Thyroid Cancer and Thyroid Disease. *Epidemiology* **2010**, *21*, 389–395.

(10) Tajtáková, M.; Semanová, Z.; Tomková, Z.; Szökeová, E.; Majoroš J.; Rádiková, Z.; Šeböková, E.; Klimeš, I.; Langer, P. Increased

Thyroid Volume and Frequency of Thyroid Disorders Signs in Schoolchildren from Nitrate Polluted Area. *Chemosphere* **2006**, *62*, 559–564.

(11) Jones, R. R.; Weyer, P. J.; DellaValle, C. T.; Inoue-Choi, M.; Anderson, K. E.; Cantor, K. P.; Krasner, S.; Robien, K.; Freeman, L. E. B.; Silverman, D. T.; Ward, M. H. Nitrate from Drinking Water and Diet and Bladder Cancer Among Postmenopausal Women in Iowa. *Environ. Health Perspect.* **2016**, *124*, 1751–1758.

(12) Espejo-Herrera, N.; Cantor, K. P.; Malats, N.; Silverman, D. T.; Tardón, A.; García-Closas, R.; Serra, C.; Kogevinas, M.; Villanueva, C. M. Nitrate in Drinking Water and Bladder Cancer Risk in Spain. *Environ. Res.* **2015**, *137*, 299–307.

(13) Chiu, H.; Tsai, S.; Yan, C. Nitrate in Drinking Water and Risk of Death from Bladder Cancer: An Ecological Case-Control Study in Taiwan. *J. Toxicol. Environ. Health* **2007**, *70*, 1000–1004.

(14) Temkin, A.; Evans, S.; Manidis, T.; Campbell, C.; Naidenko, O. V. Exposure-Based Assessment and Economic Valuation of Adverse Birth Outcomes and Cancer Risk Due to Nitrate in United States Drinking Water. *Environ. Res.* **2019**, *176*, 108442.

(15) Lundberg, J. O.; Weitzberg, E.; Cole, J. A.; Benjamin, N. Nitrate, Bacteria and Human Health. *Nat. Rev. Microbiol.* **2004**, *2*, 594–602.

(16) Wang, M.; Hu, C.; Barnes, B. B.; Mitchum, G.; Lapointe, B.; Montoya, J. P. The Great Atlantic Sargassum Belt. *Science* **2019**, *365*, 83–87.

(17) Des Moines Waterworks' 2015 Denitrification Record, http://www.dmww.com/about-us/news-releases/des-moines-water-works-2015-denitrification-record.aspx (accessed Nov. 21, 2018).

(18) Barrabés, N.; Sá, J. Catalytic Nitrate Removal from Water, Past, Present and Future Perspectives. *Appl. Catal. B* **2011**, *104*, 1–5.

(19) Martínez, J.; Ortiz, A.; Ortiz, I. State-Of-The-Art and Perspectives of the Catalytic and Electrocatalytic Reduction of Aqueous Nitrates. *Appl. Catal. B* **2017**, *207*, 42–59.

(20) Bae S.; Stewart, K. L.; Gewirth, A. A. Nitrate Adsorption and Reduction on Cu(001) in Acidic Solution. *J. Am. Chem. Soc.* **2007**, *129*, 10171–10180.

(21) Sakamoto, Y.; Nakata, K.; Kamiya, Y.; Okuhara, T. Cu-Pd Bimetallic Cluster/AC as a Novel Catalyst for the Reduction of Nitrate to Nitrite. *Chem. Lett.* **2004**, *33*, 908–909.

(22) Guo, S.; Heck, K.; Kasiraju, S.; Qian, H.; Zhao, Z.; Grabow, L. C.; Miller, J. T.; Wong, M. S. Insights into Nitrate Reduction over Indium-Decorated Palladium Nanoparticle Catalysts. *ACS Catal.* **2018**, *8*, 503–515.

(23) Mikami, I.; Yoshinaga, Y.; Okuhara, T. Rapid Removal of Nitrate in Water by Hydrogenation to Ammonia with Zr-Modified Porous Ni Catalysts. *Appl. Catal. B* **2004**, *49*, 173–179.

(24) Shukla, A.; Pande, J. V.; Bansiwal, A.; Osiceanu, P.; Biniwale, R. B. Catalytic Hydrogenation of Aqueous Phase Nitrate over Fe/C Catalysts. *Catal. Lett.* **2009**, *131*, 451–457.

(25) Rai, R. K.; Tyagi, D.; Singh, S. K. Room-Temperature Catalytic Reduction of Aqueous Nitrate to Ammonia with Ni Nanoparticles Immobilized on an Fe_3O_4@n-SiO_2@h-SiO_2-NH_2 Support. *Eur. J. Inorg. Chem*. **2017**, 2450–2456.

(26) Liou, Y. H.; Lin, C. J.; Hung, I. C.; Chen S. Y.; Lo, S. L. Selective Reduction of NO_3^- to N_2 with Bimetallic Particles of Zn Coupled with Palladium, Platinum, and Copper. *Chem. Eng. J.* **2012**, *181–182*, 236–242.

(27) Soares, O. S. G. P.; Órfão, J. J. M.; Pereira, M. F. Activated Carbon Supported Metal Catalyst for Nitrate and Nitrite Reduction in Water. *Catal. Lett*. **2008**, *126*, 253–260.

(28)Majumdar, A.; Pal, K.; Sarkar, S. Chemistry of $[Et_4N][Mo^{IV}(SPh)(PPh_3)(mnt)_2]$ as an Analogue of Dissimilatory nitrate Reductase with Its Inactivation on Substitution of Thiolate by Chloride. *J. Am. Chem. Soc.* **2006**, *128*, 4196–4197.

(29) Xu, S.; Ashley, D. C.; Kwon, H.; Ware, G. R.; Chen, C.; Losovyj, Y.; Gao, X.; Jakubikova, E.; Smith, J. M. A Flexible, Redox-Active Macrocycle Enables the Electrocatalytic Reduction of Nitrate to Ammonia by a Cobalt Complex. *Chem. Sci.* **2018**, *9*, 4950–4958.

(30) Ford, C. L.; Park, Y. J.; Matson, E. M.; Gordon, Z.; Fout, A. R. A Bioinspired Iron Catalyst for Nitrate and Perchlorate Reduction. *Science* **2016**, *354*, 741–743.

(31) Popczun, E. J.; McKone, J. R.; Read, C. G.; Biacchi, A. J.; Wiltrout, A. M.; Lewis, N. S.; Schaak, R. E. Nanostructured Nickel Phosphides as an Electrocatalyst for the Hydrogen Evolution Reaction. *J. Am. Chem. Soc.* **2013**, *135*, 9267–9270.

(32) Callejas, J. F.; Read, C. G.; Roske, C. W.; Lewis, N. S.; Schaak, R. E. Synthesis, Characterization, and Properties of Metal Phosphide Catalysts for the Hydrogen-Evolution Reaction. *Chem. Mater.* **2016**, *17*, 6017–6044.

(33) Feng, L.; Xue, H. Advances in Transition-Metal Phosphide Applications in Electrochemical Energy Storage and Catalysis. *ChemElectroChem* **2017**, *4*, 20–34.

(34) Xiao, P.; Chen, W.; Wang, X. A Review of Phosphide-Based Materials for Electrocatalytic Hydrogen Evolution. *Adv. Energy Mater.* **2015**, *5*, 1500985.

(35) Liu, P.; Rodriguez, J. A. Catalysts for Hydrogenation Evolution from the [NiFe] Hydrogenase to the Ni_2P(001) Surface: The Importance of Ensemble Effect. *J. Am. Chem. Soc*. **2005**, *127*, 14871–14878.

(36) Andaraarachchi, H. P.; Thompson, M. J.; White, M. A.; Fan, H.; Vela, J. Phase-Programmed Nanofabrication: Effect of Organophosphite Precursor Reactivity on the Evolution of Nickel and Nickel Phosphide Nanocrystals. *Chem. Mater.* **2015**, *27,* 8021–8031.

(37) Owens-Baird, B.; Kolen'ko, Y. V.; Kovnir, K. Structure–Activity Relationships for Pt-Free Metal Phosphide Hydrogen Evolution Electrocatalysts. *Chem. Eur. J.* **2018**, *24*, 7298–7311.

(38) Mora-Tamez, L.; Barim, G.; Downes, C.; Williamson, E. M.; Habas, S. E.; Brutchey, R. L. Controlled Design of Phase- and Size-Tunable Monodisperse Ni_2P Nanoparticles in a Phosphonium-Based Ionic Liquid through Response Surface Methodology. *Chem. Mater*. **2019**, *31*, 1552–1560.

(39) Savithra, G. H. L.; Muthuswamy, E.; Bowker, R. H.; Carrillo, B. A.; Bussell, M. E.; Brock, S. L. Rational Design of Nickel Phosphide Hydrodesulfurization Catalysts: Controlling Particle Size and Preventing Sintering. *Chem. Mater.* **2013**, *25*, 825–833.

(40) Prins, R.; Bussell, M. E. Metal Phosphides: Preparation, Characterization and Catalytic Reactivity. *Catal. Lett.* **2012**, *142*, 1413–1436.

(41) Oyama, S. T. Novel Catalysts for Advanced Hydroprocessing: Transition Metal Phosphides. J. Catal. 2003, 216, 343–352.

(42) Carenco, S.; Boissière, C.; Mézailles, N.; Sanchez, C. Metal phosphides: A Revival at the Nanoscale. *Actual. Chimique* **2012**, *362*, 22–28.

(43) Yang, Y.; Ochoa-Hernández, C.; de la Peña O'Shea, V. A.; Coronado, J. M.; Serrano, D. P. Ni_2P/SBA-15 as a Hydrodeoxygenation Catalyst with Enhanced Selectivity for the Conversion of Methyl Oleate into n-Octadecane. *ACS Catal.* **2012**, *2*, 592–598.

(44) Lu, M.; Zheng, L.; Li, M.; Guan, Q.; Li, W. Efficient Hydrogenation Performance Improvement of MoP and Ni_2P Catalysts by Adjusting the Electron Distribution Around Mo and Ni Atoms. *RSC Adv.* **2016**, *6*, 65081–65088.

(45) Zhao, H. Y.; Li, D.; Bui, P.; Oyama, S. T. Hydrodeoxygenation of Guaiacol as Model Compound for Pyrolysis Oil on Transition Metal Phosphide Hydroprocessing Catalysts. *Appl. Catal. A* **2011**, *391*, 305–310.

(46) Lu, M.; Wang, A.; Li, X.; Duan, X.; Teng, Y.; Wang, Y.; Song, C.; Hu, Y. Hydrodenitrogenation of Quinoline Catalyzed by MCM-41-Supported Nickel Phosphides. *Energy Fuels* **2007**, *21*, 554–560.

(47) Robinson, W. R. A. M.; van Gestel, J. N. M.; Korányi, T. I.; Eijsbouts, S.; van der Kraan, A. M.; van Veen, J. A. R.; de Beer, V. H. J. Phosphorus Promotion of Ni(Co)-Containing Mo-Free Catalysts in Quinoline Hydrodenitrogenation. *J. Catal.* **1996**, *161*, 539–550.

(48) Delley, M. F.; Wu, Z.; Mundy, M. E.; Ung, D.; Cossairt, B. M.; Wang, H.; Mayer, J. M. Hydrogen on Cobalt Phosphide. *J. Am. Chem. Soc.* **2019**, *141*, 15390–15402.

(49) Carenco, S.; Levya-Pèrez, A.; Concepcion, P.; Boissière, C.; Mézailles, N.; Sanchez, C.; Corma, A. Nickel Phosphide Nanocatalysts for the Chemoselective Hydrogenation of Alkynes. *Nano Today* **2012**, *7*, 21–28.

(50) Chen, Y.; Changmin, L.; Zhou. J.; Zhang, S.; Rao, D.; He, S.; Wei, M.; Evans, D. G.; Duan, X. Metal Phosphides Derives from Hydrotalcite Precursors toward the Selective Hydrogenation of Phenylacetylene. *ACS Catal.* **2015**, *5*, 5756–5765.

(51) Shamanaev, I. V.; Deily, I. V.; Aleksandrov, P. V.; Gerasimov, E. U.; Pakharukova, V. P.; Kodnev, E. G.; Ayupov, A. B.; Andreev, A. S.; Lapina, O. B.; Bukhtiyarova, G. A. Effect of Precursor on the Catalytic Properties of Ni_2P/SiO_2 in Methyl Palmitate Hydrodeoxygenation. *RSC Adv.* **2016**, *6*, 30372–30383.

(52) Yun, G.; Guan, Q.; Li. W. The Synthesis and Mechanistic Studies of a Highly Active Nickel Phosphide Catalyst for Naphthalene Hydrodearomatization. *RSC Adv.* **2017**, *7*, 8677–8687.

(53) Roberts, E. J.; Read C. G.; Lewis, N. L.; Brutchey, R. L. Phase Directing Ability of an Ionic Liquid Solvent for the Synthesis of HER-Active Ni_2P Nanocrystals. *ACS Appl. Energy Mater*. **2018**, *1*, 1823–1827.

(54) Senevirathne, K.; Burns, A. W.; Bussell, M. E.; Brock, S. L. Synthesis and Characterization of Discrete Nickel Phosphide Nanoparticles: Effect of Surface Ligation Chemistry on Catalytic Hydrodesulfurization of Thiophene. *Adv. Funct. Mater*. **2007**, *17*, 3933–3939.

(55) Pan, Y.; Liu, Y.; Zhao, J.; Yang, K.; Liang, J.; Liu, D.; Hu, W.; Liu, D.; Liu, Y.; Liu, C. Monodispersed Nickel Phosphide Nanocrystals with Different Phases: Synthesis, Characterization and Electrocatalytic Properties for Hydrogen Evolution. *J. Mater. Chem. A* **2015**, *3*, 1656–1665.

(56) *XRD Standard Patterns*; Inorganic Crystal Structure Database: Karlsruhe, Germany, 2019.

(57) Popczun, E. J.; Read, C. G.; Roske, C. W.; Lewis, N. S.; Schaak, R. E. Highly Active Electrocatalysis Reaction by Cobalt Phosphide Nanoparticles. *Angew. Chem. Int. Ed.* **2014**, *53*, 5427–5430.

(58) *National Primary Drinking Water Regulations*, EPA-F-09-004, United States Environmental Protection Agency: Washington, DC., 2009.

(59) World Health Organization. *Guidelines for Drinking-Water Quality*: *Fourth Edition Incorporating the First Addendum*; Geneva, 2017; 398.

(60) Yoshinaga, Y.; Akita, T.; Mikami, I.; Okuhara, T. Hydrogenation of Nitrate in Water to Nitrogen over Pd-Cu Supports on Active Carbon. *J Catal*. **2002**, *207*, 37–45.

(61) Jafarinejad, S.; Park, H.; Mayton, H.; Walker, S. L; Jiang, S. C. Concentrating Ammonium in Wastewater by Forward Osmosis using a Surface Modified Nanofiltration Membrane. *Environ. Sci.: Water Res. Technol*. **2019**, *5*, 246–255.

(62) Cancino-Madariaga, B.; Hurtado, C. F.; Ruby, R. Effect of Pressure and pH in Ammonium Retention for Nanofiltration and Reverse Osmosis Membranes to be used in Recirculation Aquaculture Systems (RAS). *Aquacult. Eng*. **2011**, *45*, 103–108.

(63) Huang, A. H.; Liu, J. C. Removal of Ammonium as Struvite from Wet Scrubber Wastewater. *Water Air Soil Pollut.* **2014**, *225*, 2062–2070.

(64) Huang, J.; Kankanamge, N. R.; Chow, C.; Welsh, D. T.; Li, T.; Teasdale, P. R. Removing Ammonium from Water and Wastewater using Cost-Effective Adsorbents: A Review. *J. Environ. Sci.* **2018**, *63*, 174–197.

(65) Huang, J.; Kankanamge, N. R.; Chow, C.; Welsh, D. T.; Li, T.; Teasdale, P. R. Removing Ammonium from Water and Wastewater Using Cost-Effective Adsorbents: A Review. *J. Environ. Sci.* **2018**, *63*, 174–197.

(66) *Fertilizer Use and Price*, U.S. Department of Agriculture Economic Research Service, Washington DC., 2018.

(67) Erisman, J. W.; Sutton, M. A; Galloway, J.; Klimont, Z.; Winiwarter, W. How a Century of Ammonia Synthesis Changed the World. *Nat. Geosci*. **2008**, *1*, 636–639.

(68) Laursen, A. B.; Patraju, K. R.; Whitaker, M. J.; Retuerto, M.; Sarkar, T.; Yao, N.; Ramanujachary, K. V.; Greenblatt, M.; Dismukes, G.C. Nanocrystalline Ni_5P_4: A Hydrogen Evolution Electrocatalyst of Exceptional Efficiency in Both Alkaline and Acidic Media. *Energy Environ. Sci.* **2015**, *8*, 1027–1034.

(69) Kandegedara, A.; Rorabacher, D. B. Noncomplexing Tertiary Amines as "Better" Buffers Covering the Range of pH 3-11. Temperature Dependence of Their Acid Dissociation Constants. *Anal. Chem.* **1999**, *71*, 3140–3144.

(70) Wärn, J.; Turunen, I.; Salmi, T.; Maunula, T. Kinetics of Nitrate Reduction in Monolith Reactor. *Chem. Eng. Sci.* **1994**, *49*, 5763–5773.

(71) Pintar, A.; Batista, J.; Levec, J. Potential of Mono- and Bimetallic Catalysts for Liquid-Phase Hydrogenation of Aqueous Nitrite Solutions. *Water Sci. Technol.* **1998**, *37*, 177–185.

(72) Brunet Espinosa, R.; Lefferts, L Ni in CNFs: Highly Active for Nitrite Hydrogenation. *ACS Catal*. **2016**, *6*, 5432–5440.

(73) Seraj, S.; Kunal, P. Li, H.; Henkelman, G.; Humphrey, S. M.; Werth, C. J. PdAu Alloy Nanoparticle Catalysts: Effective Candidates for Nitrite Reduction in Water. *ACS Catal.* **2017**, *7*, 3268–3276.

(74) Huo, X.; Van Hoomisen, D. J.; Liu, J.; Vyas, S.; Strathmann, T. J. Hydrogenation of Aqueous Nitrate and Nitrite with Ruthenium Catalysts. *Appl. Catal. B* **2017**, *211*, 188–198.

(75) Gadzhiev, O. B.; Ignatov, S. K.; Gangopadhyay, S.; Masunov, A. E.; Petrov, A. I. Mechanism of Nitric Oxide Oxidation Reaction ($2NO + O_2 \rightarrow 2NO_2$) Revisited. *J. Chem. Theory Comput*. **2011**, *7*, 2021–2024.

(76) Lewis, R. S.; Deen, W. M. Kinetics of the Reaction of Nitric Oxide with Oxygen in Aqueous Solutions. *Chem. Res. Toxicol*. **1994**, *7*, 568–574.

(77) *NIST X-ray Photoelectron Spectroscopy Database*: srdata.nist.gov/xps/ (accessed Aug 24, 2019).

(78) Biesinger, M. C.; Payne, B. P.; Lau, L. W. M.; Gerson, A.; Smart R. St. C.; X-Ray Photoelectron Spectroscopic Chemical State Quantification of Mixed Nickel Metal, Oxide and Hydroxide Systems. *Surf. Interface. Anal.* **2009**, *41*, 324–332.

(79) Nelson, N. C.; Ruberu, T. P. A.; Reichert, M. D.; Vela, J. Templated Synthesis and Chemical Behavior of Nickel Nanoparticles within High Aspect Ratio Silica Capsules. *J. Phys. Chem. C* **2013**, *117*, 25826–25836.

(80) Pannu, S. S. Nitric Acid. *J. Chem. Educ*. **1984**, *61*, 174–176.

(81) Carenco, S.; Boissière, C.; Nicole, L.; Sanchez, C.; Le Floch, P.; Mézailles, N. Controlled Design of Size-Tunable Monodisperse Nickel Nanoparticles. *Chem. Mater*. **2010**, *22*, 1340–1349.

(82) Kresse, G.; Hafner, J. Ab initio Molecular Dynamics for Liquid Metals. *Phys. Rev. B* **1993**, *47*, 558–561.

(83) Kresse, G.; Hafner, J. Ab initio Molecular-Dynamics Simulation of the Liquid-Metal-Amorphous-Semiconductor Transition in Germanium. *Phys. Rev. B* **1994**, *49*, 14251–14269.

(84) Blöchl, P. E. Porjector Augmented-Wave Method. *Phys. Rev. B* **1994**, *50*, 17953–17979.

(85) Kresse, G.; Joubert, D. From Ultrasoft Pseudopotentials to the Projector Augmented-Wave Method. *Phys. Rev. B* **1999**, *59*, 1758–1775.

(86) Perdew, J. P.; Burke, K.; Ernzerhof, M. Generalized Gradient Approximation Made Simple. *Phys. Rev. Lett.* **1996**, *77*, 3865–3868.

(87) Mathew K.; Hennig, R. G. VASPsol-Solvation Model for the Plane Wave DFT Code VASP. https://github.com/henniggroup/VASPsol (2015) (accessed Sep 4, 2019).

TOC Figure